

On the Stability of the Soft Pendulum With Affine Curvature: Open-Loop, Collocated Closed-Loop, and Switching Control

Maja Trumić^{1b}, Graduate Student Member, IEEE, Cosimo Della Santina^{2b}, Member, IEEE, Kosta Jovanović^{1b}, Member, IEEE, and Adriano Fagiolini^{2b}, Member, IEEE

Abstract—This letter investigates the stability properties of the soft inverted pendulum with affine curvature - a template model for nonlinear control of underactuated soft robots. We look at how changes in physical parameters affect stability and equilibrium. We give conditions under which zero dynamics corresponding to a collocated choice of the output is (locally or globally) stable or unstable. We leverage these results to design a switching controller that stabilizes a class of nonlinear equilibria of the pendulum, which can drive the system from one equilibrium to another.

Index Terms—Emerging control applications, stability of nonlinear systems, robotics.

I. INTRODUCTION

CONTINUUM soft robots are nature-inspired mechanical systems [1] entirely made of continuously deformable materials. This feature gives them morphological flexibility so their body can swirl, twist, and bend in space. However, these capabilities come at the price of a substantially more complex control problem. Many researchers have resorted to machine learning and model-free strategies to solve the challenge of controlling these systems [2].

On the other hand, research in soft robot modeling has shown that simple yet accurate models [3], can lead to a breakthrough in applying model-based control approaches [4]. While the initial research stream has mainly been oriented toward the kinematic control of soft robots [5], this trend later expanded to dynamic control by artificially casting the

problem as fully actuated [6]–[8]. Nevertheless, this approach requires imposing coarse approximations. Indeed, the high (theoretically infinite) dimensionality of soft robots' dynamics makes any accurate description inherently underactuated. Thus, naturally, control of underactuated soft robots is attracting a growing amount of attention nowadays. Linear approximations have proven to be a feasible solution when aiming for local results [9], [10]. Moving to the nonlinear case, most of the existing approaches work under the (sometimes implicit) assumption that the soft robot is *stiff-enough*. Examples are the PD-poly in [11], the computed torque plus zero-dynamics damping injection in [12], the PD+ in [13], and the energy shaping controllers in [14]–[16]. Recently, two template models for soft robots have been proposed: the soft pendulum with a revolute base [17] and the soft inverted pendulum (SIP) with affine curvature [18]. The former is a soft version of the double pendulum and the latter of the acrobot [19]. The ultimate goal is to follow a similar path of nonlinear control of underactuated rigid robots: to relax hypotheses by focusing on specific, low-dimensional, but representative systems. Energy-based control and feedback linearization are investigated [17], [18]. Beyond the initial results, a complete understanding of the behaviors of these template models is far from being achieved.

In this letter, we dig into the essential characteristics of the SIP, towards a more comprehensive understanding of its structural properties. We expand the analysis in [18] and focus on how the robot's physical parameters impact the number of equilibria, potential energy, and collocated zero-dynamics stability. With respect to [18], we also provide analytic results and perform numerical characterizations regarding the local and global stability, and the instability of the zero dynamics for different values of the collocated component. We propose an energy-injection switching control strategy that allows the transition from one open-loop unstable equilibrium to another one, sharing the same collocated variable, or among equilibria with different collocated components. This controller is inspired by the swing-up control strategy used in classic pendulum systems [20]. We envision this analysis may serve during the design of a soft robot as a guideline to ensure the existence of a single equilibrium, e.g., in a soft neck, or of several ones when the robot has to manipulate objects by spiralling around them or to move with constant tip orientation. Units are omitted in this letter for brevity reasons. Angles are in radians and all other quantities are in the units of the MKS system.

II. THE SOFT INVERTED PENDULUM MODEL

We report here a succinct introduction to the dynamic model of an inextensible SIP with affine curvature. An interested

Manuscript received 21 March 2022; revised 29 May 2022; accepted 15 June 2022. Date of publication 30 June 2022; date of current version 18 July 2022. This work was supported in part by the Science Fund of the Republic of Serbia, PROMIS (ForNextCobot) under Grant 6062528. Recommended by Senior Editor L. Zhang. (Corresponding author: Adriano Fagiolini.)

Maja Trumić is with the School of Electrical Engineering, University of Belgrade, 11000 Belgrade, Serbia, and also with the Mobile & Intelligent Robots @ Panormous Laboratory, Department of Engineering, University of Palermo, 90128 Palermo, Italy (e-mail: maja.trumic@etf.rs).

Cosimo Della Santina is with the Department of Cognitive Robotics, Delft University of Technology, 2628 CD Delft, The Netherlands, and also with the Institute of Robotics and Mechatronics, German Aerospace Center, 51147 Cologne, Germany (e-mail: c.dellasantina@tudelft.nl).

Kosta Jovanović is with the School of Electrical Engineering, University of Belgrade, 11000 Belgrade, Serbia (e-mail: kostaj@etf.rs).

Adriano Fagiolini is with the Mobile & Intelligent Robots @ Panormous Laboratory, Department of Engineering, University of Palermo, 90128 Palermo, Italy (e-mail: fagiolini@unipa.it).

Digital Object Identifier 10.1109/LCSYS.2022.3187612

2475-1456 © 2022 IEEE. Personal use is permitted, but republication/redistribution requires IEEE permission.
See <https://www.ieee.org/publications/rights/index.html> for more information.

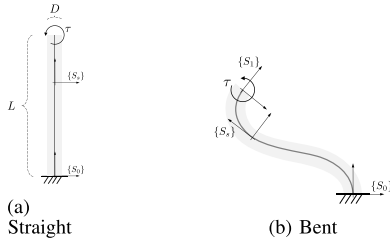


Fig. 1. This letter analyzes the structural properties of the soft pendulum with affine curvature, with a special focus on collocated control. This template model has two degrees of freedom and one degree of actuation, and it presents a soft version of the rigid acrobot.

reader can refer to [18] for an in-depth description of this template model. Referring to Fig. 1, consider a soft-bodied robot consisting of a SIP, i.e., a flexible cylinder-shaped segment with a total length L , a width D , and a damping β , attached to the ground. Let $s \in [0, 1]$ be a first local coordinate parametrizing all points of the pendulum's central axis. We define it as the normalized arc length of the curve going from the base to the point of interest, so that the base corresponds to $s = 0$ and the tip to $s = 1$. Let $d \in [-\frac{1}{2}, \frac{1}{2}]$ be a second local coordinate parametrizing all points within the pendulum's cross section, so that $d = 0$ is the central axis and $d = \pm\frac{1}{2}$ are the outer parts. Let $\rho(s, d)$ and $k^*(s, d)$ be the local mass and stiffness, respectively, and the total mass be $m = \int_0^1 \int_{-\frac{1}{2}}^{\frac{1}{2}} \rho(s, d) dd ds$. Assume the robot's curvature is affine in s , i.e., $\mu_s(t) = (1, s)\theta(t) = \theta_0(t) + \theta_1(t)s$, where $\theta = (\theta_0, \theta_1)^T$ is its configuration vector. An external input torque τ can be applied at its tip, while the whole system is subject to the gravity force. The SIP dynamics reads $\tilde{B}(\theta)\ddot{\theta} + \tilde{C}(\theta, \dot{\theta})\dot{\theta} + \tilde{G}(\theta) + kH\theta + \beta H\dot{\theta} = H(\tau, 0)^T$, with $\tilde{B}, \tilde{C} \in \mathbb{R}^{2 \times 2}$ being the inertia matrix and the matrix collecting Coriolis and centrifugal terms, respectively, $\tilde{G} \in \mathbb{R}^2$ the gravity vector, and $H = \begin{pmatrix} 1 & 1/2 \\ 1/2 & 1/3 \end{pmatrix}$ is a Hankel matrix [18].

The coordinate change $q = (q_0, q_1)^T = H\theta$ allows separating the actuated and unactuated dynamics as:

$$B(q)\ddot{q} + C(q, \dot{q})\dot{q} + G(q) + Kq + \Delta\dot{q} = (\tau, 0)^T \quad (1)$$

where $B(q) = H^{-1}\tilde{B}(H^{-1}q)H^{-1}$ is positive definite and bounded, $C(q, \dot{q}) = H^{-1}\tilde{C}(H^{-1}q, H^{-1}\dot{q})H^{-1}$ is chosen so that $\dot{B}(q) - 2C(q, \dot{q})$ is skew-symmetric, $K = H^{-1}k$, $\Delta = H^{-1}\beta$, and $G(q) = H^{-1}\tilde{G}(H^{-1}q)$. We assume here that G and $\partial G/\partial q$ are bounded, which can be verified numerically over large domains of q . Moreover, B , C , and G are continuously differentiable in all their input arguments. Defining the orientation angle $\alpha_s = \int_0^s \mu_v(t) dv$ allows giving a physical meaning to the newly-introduced coordinates. Namely, $q_0 = \theta_0 + \frac{1}{2}\theta_1 = \alpha_1$ is the tip orientation and $q_1 = \frac{1}{2}\theta_0 + \frac{1}{3}\theta_1 = \int_0^1 \alpha_s ds$ is the average orientation.

III. A STUDY OF EQUILIBRIA AND POTENTIAL ENERGY

The first peculiarity of a SIP stems from the number of possessed equilibria. While a rigid double pendulum has always a stable downward equilibrium and an unstable upward one, a SIP may have many equilibria with parameter-dependent stability. To delve into this feature, we consider its potential energy and study the equilibria and their stability. In doing this, we focus on mass distributions of the form

$$\rho(s, d) = m_0(1 + \kappa) + \sum_{i=1}^{\kappa} (m_i - m_0) \delta(s - s_i, d) \quad (2)$$

where $m_i = m\sigma_i$, $\sigma_i \in (0, 1]$ is the i -th local mass proportion with respect to the total mass m , $\sum_{i=0}^{\kappa} \sigma_i = 1$, and $\delta(s, d)$ is a Dirac's delta. This form is quite general and allows describing uniform distributions, discrete distributions of κ lumped masses m_i located along the SIP's central axis, i.e., at $s = s_i$ and $d = 0$, or their combinations. For a uniform mass distribution it holds $\rho(s, d) = m_0$ for all s, d and $m = m_0$ as the SIP's volume $\int_0^1 \int_{-\frac{1}{2}}^{\frac{1}{2}} dd ds$ is unitary. In the general case, direct calculations show, as expected, that $m = \int_0^1 \int_{-\frac{1}{2}}^{\frac{1}{2}} m_0(1 + \kappa) dd ds + \sum_{i=1}^{\kappa} ((m_i - m_0) \int_0^1 \int_{-\frac{1}{2}}^{\frac{1}{2}} \delta(s - s_i, d) dd ds) = \sum_{i=0}^{\kappa} m_i$.

A. Potential Energy

The number of equilibria of a mechanical system is mapped to that of (local) minima of its potential energy. A major feature distinguishing the SIP from its rigid counterpart stems in the form of its potential energy. Such energy is the sum of the gravity potential energy U_G and the elastic potential energy U_K , i.e., $U = U_G + U_K$, each summing all infinitesimal contributions as below:

$$\begin{aligned} U_G &= \int_0^1 \int_{-\frac{1}{2}}^{\frac{1}{2}} \rho(s, d) g (x_{s,d}(q)s_\phi + y_{s,d}(q)c_\phi) dd ds \\ U_K &= \int_0^1 \int_{-\frac{1}{2}}^{\frac{1}{2}} \frac{1}{2} k^*(s, d) q^T H^{-1} q dd ds \end{aligned} \quad (3)$$

where $(x_{s,d}(q), y_{s,d}(q))$ is the Cartesian coordinate of a generic point (s, d) moving along the SIP, $s_\phi = \sin \phi$, $c_\phi = \cos \phi$, with $\phi \in [0, 2\pi]$ being the angle that the base of the robot has w.r.t. the gravity field. Interestingly, U_G can be conveniently factorized so as to extract all geometric and inertial parameters. Recall first from [18] that $x_{s,d}(q) = Lx'_s(q) + dD \cos(\theta_0 + \theta_1 s^2/2)$ and $y_{s,d}(q) = Ly'_s(q) + dD \sin(\theta_0 + \theta_1 s^2/2)$, with D the SIP's width, $\theta_0 = 4q_0 - 6q_1$, $\theta_1 = -6q_0 + 12q_1$, and $x'_s(q)$ and $y'_s(q)$ being independent of L . Then, it stands:

Proposition 1: For all mass distributions as in (2), it holds

$$U_G = mgL \left(\sigma_0(1 + \kappa) \int_0^1 p_s(q) ds + \sum_{i=1}^{\kappa} (\sigma_i - \sigma_0) p_{s_i}(q) \right),$$

where $p_s(q) = x'_s(q)s_\phi + y'_s(q)c_\phi$.

Proof: Plugging (2) into U_G yields

$$\begin{aligned} U_G &= mg \left(\sigma_0(1 + \kappa) \int_0^1 \int_{-\frac{1}{2}}^{\frac{1}{2}} v_{s,d}(q) dd ds \right. \\ &\quad \left. + \sum_{i=1}^{\kappa} (\sigma_i - \sigma_0) \int_0^1 \int_{-\frac{1}{2}}^{\frac{1}{2}} v_{s,d}(q) \delta_i dd ds \right), \end{aligned}$$

with $v_{s,d}(q) = x_{s,d}(q)s_\phi + y_{s,d}(q)c_\phi$ and $\delta_i = \delta(s - s_i, d)$. Expanding the expressions of $x_{s,d}(q)$ and $y_{s,d}(q)$ one gets $\int_{-\frac{1}{2}}^{\frac{1}{2}} (x_{s,d}(q)s_\phi + y_{s,d}(q)c_\phi) dd = Lp_s(q)$, by observing that the addends depending on d vanish as they are odd functions integrated over symmetrical intervals. Moreover, using the shifting property of Dirac's delta and the relations $x_{s,0}(q) = Lx'_s(q)$ and $y_{s,0}(q) = Ly'_s(q)$, the second addend in the above expression of U_G can be simplified as $\sum_{i=1}^{\kappa} (\sigma_i - \sigma_0) (x_{s_i,0} s_\phi + y_{s_i,0} c_\phi) = L \sum_{i=1}^{\kappa} (\sigma_i - \sigma_0) p_{s_i}(q)$. Putting all together leads to U_G 's expression in the statement. ■

Moreover, U_K can also be factorized as follows:

Proposition 2: For a SIP with local stiffness $k^*(s, d)$, it holds $U_K = kq^T H^{-1} q$, where $k = \int_0^1 \int_{-\frac{1}{2}}^{\frac{1}{2}} \frac{1}{2} k^*(s, d) dd ds$ is the SIP's average stiffness.

Proof: Observing that $q^T H^{-1} q$ is constant in s and d , the property immediately follows from U_K 's definition. ■

B. Equilibrium Pattern and Local Stability

Given a constant input torque $\bar{\tau}$, an equilibrium pair (\bar{q}_0, \bar{q}_1) of a SIP consists of constant solutions $q_0(t) = \bar{q}_0$, $q_1(t) = \bar{q}_1$ of (1) for $\tau = \bar{\tau}$ and $\dot{q}_0 = \dot{q}_1 = \ddot{q}_0 = \ddot{q}_1 = 0$. It satisfies the equilibrium conditions:

$$\begin{aligned} G_1(\bar{q}_0, \bar{q}_1) + K_{1,1}\bar{q}_0 + K_{1,2}\bar{q}_1 &= \bar{\tau} \\ G_2(\bar{q}_0, \bar{q}_1) + K_{2,1}\bar{q}_0 + K_{2,2}\bar{q}_1 &= 0 \end{aligned} \quad (4)$$

where G_i is the i -th component of G . Due to the complexity of G_1 and G_2 , the equilibrium pairs (\bar{q}_0, \bar{q}_1) solving (4) cannot be obtained in closed form and must be determined numerically. Examples of their shapes are graphically presented in [1]. We analyze here their stability, which can be done by looking at the definiteness of the stiffness matrix as suggested in Theorem 1 from [4]:

$$\mathcal{K}(\bar{q}_0, \bar{q}_1) = \nabla_q(G(q) + Kq)|_{q=(\bar{q}_0, \bar{q}_1)}. \quad (5)$$

Namely, an equilibrium pair (\bar{q}_0, \bar{q}_1) of the SIP is asymptotically stable if, and only if, the matrix $\mathcal{K}(\bar{q}_0, \bar{q}_1)$ is positive definite, which can be studied, e.g., via Sylvester's criterion. Towards this goal, using Prop. 1, the gravity vector can be factorized as $G(q) = \nabla_q^T U_G(q) = mgL \Gamma(q)$, with

$$\Gamma(q) = \nabla_q^T \left(\sigma_0(1 + \kappa) \int_0^1 p_s(q) ds + \sum_{i=1}^{\kappa} (\sigma_i - \sigma_0) p_{s_i}(q) \right)$$

and hence, at the equilibrium pair, it holds $G_i(\bar{q}_0, \bar{q}_1) = mgL \Gamma_i(\bar{q}_0, \bar{q}_1)$, for $i = 1, 2$, and the boundedness of Γ and $\partial\Gamma/\partial q$ are inherited from those of G and $\partial G/\partial q$. Then, using the relations $K_{1,1} = 4k$, $K_{1,2} = K_{2,1} = -6k$ and $K_{2,2} = 12k$, where $K_{i,j}$ are the components of K in (1), (4) is rewritten as

$$mgL \begin{pmatrix} \Gamma_1(\bar{q}_0, \bar{q}_1) + \gamma(4\bar{q}_0 - 6\bar{q}_1) \\ \Gamma_2(\bar{q}_0, \bar{q}_1) + \gamma(12\bar{q}_1 - 6\bar{q}_0) \end{pmatrix} = \begin{pmatrix} \bar{\tau} \\ 0 \end{pmatrix} \quad (6)$$

with $\gamma = \frac{k}{mgL}$. Moreover, the stiffness matrix in (5)

is expanded as $\mathcal{K} = mgL \begin{pmatrix} \frac{\partial\Gamma_1(\bar{q}_0, \bar{q}_1)}{\partial q_0} + 4\gamma & \frac{\partial\Gamma_1(\bar{q}_0, \bar{q}_1)}{\partial q_1} - 6\gamma \\ \frac{\partial\Gamma_2(\bar{q}_0, \bar{q}_1)}{\partial q_0} - 6\gamma & \frac{\partial\Gamma_2(\bar{q}_0, \bar{q}_1)}{\partial q_1} + 12\gamma \end{pmatrix}$.

By Sylvester's criterion, \mathcal{K} is positive definite if, and only if

$$\begin{aligned} \frac{1}{mgL} \mathcal{K}_{1,1} &= \frac{\partial\Gamma_1(\bar{q}_0, \bar{q}_1)}{\partial q_0} + 4\gamma > 0 \\ \frac{1}{mgL} |\mathcal{K}| &= \left(\frac{\partial\Gamma_1}{\partial q_0} \frac{\partial\Gamma_2}{\partial q_1} - \frac{\partial\Gamma_1}{\partial q_1} \frac{\partial\Gamma_2}{\partial q_0} \right) + 12\gamma^2 \\ &+ \left(12 \frac{\partial\Gamma_1}{\partial q_0} + 4 \frac{\partial\Gamma_2}{\partial q_1} + 6 \frac{\partial\Gamma_2}{\partial q_0} + 6 \frac{\partial\Gamma_1}{\partial q_1} \right) \gamma > 0 \end{aligned} \quad (7)$$

where $mgL > 0$ and the dependency of the functions on the equilibrium pair (\bar{q}_0, \bar{q}_1) is omitted.

Noticeably, the forms of (6) and (7) reveal that the location and stability of each equilibrium depend on the ratio γ , suggesting the construction of charts illustrating their trends as a function of it. In this respect, Fig. 2 shows the sets of isolated equilibria (\bar{q}_0, \bar{q}_1) , for various values of γ with no external input ($\bar{\tau} = 0$). As in [18], we consider here a mass concentrated at the tip. The features appearing in the figure allow conjecturing the following three statements: **Conjecture 1.** *The number of equilibria increases when γ decreases, which makes γ a bifurcation parameter.* An example of this is in the rightmost plot of the figure. **Conjecture 2.** *Stable equilibria may become unstable for decreasing values of γ . If so, two stable equilibria appear in the origin's close vicinity.* This phenomenon happens for the upright position equilibrium at $(\bar{q}_0, \bar{q}_1) = (0, 0)$, which is asymptotically stable for $\gamma > \frac{13+2\sqrt{31}}{60}$ and unstable for lower values (the bifurcation value can be found by testing when Sylvester's conditions are

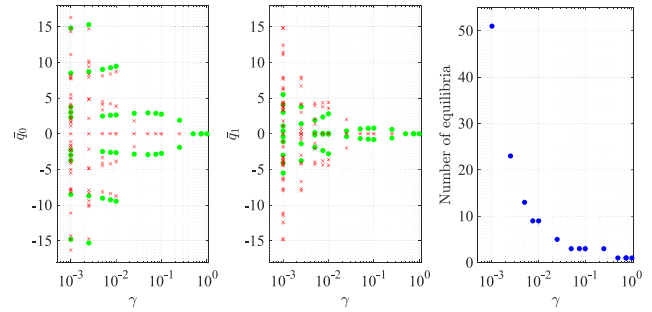


Fig. 2. Pattern, stability, and number of equilibria with no external input ($\bar{\tau} = 0$). From left to right, the first and second plots illustrate the location and stability of the equilibrium pairs (\bar{q}_0, \bar{q}_1) against the bifurcation parameter $\gamma = k/mgL$ (stable equilibria are painted in green and unstable ones are marked in red); the third plot reports the trend of the equilibrium number.

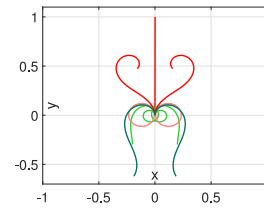


Fig. 3. Cartesian (x, y) shapes of the SIP for all equilibria existing for $\gamma = 0.01$. Green and red mark stable and unstable configurations, while color fading is used to distinguish the various configurations.

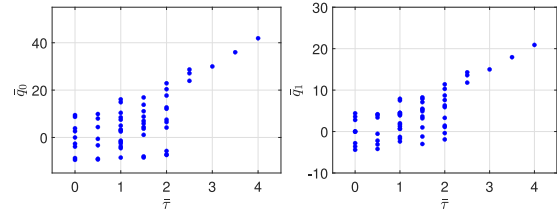


Fig. 4. Equilibrium pattern (\bar{q}_0, \bar{q}_1) for increasing values of input $\bar{\tau}$ with $\gamma = 0.01$. Large values of $\bar{\tau}$ generally reduce the number of equilibria, until only a single one remains.

not anymore met). The appearance of two new symmetrically-placed stable equilibria, in a close-by neighborhood, is a “safe” design feature, also meaning that the system exhibits supercritical pitchfork bifurcation. **Conjecture 3.** *Stable equilibria exist even for small γ .*

Moreover, Fig. 3 depicts the SIP shapes for all equilibria when $\gamma = 0.01$. By the same token, it is worth examining the effect of the external input ($\bar{\tau} \neq 0$) on the equilibrium pattern, which leads to: **Conjecture 4.** *Large input values generally reduce the equilibrium number down to a single one.* This is shown in Fig. 4. Also, relating the potential energy the following can be said: **Conjecture 5.** *For decreasing γ , two phenomena occur within the shape of potential energy: 1) new local minima appear that are separated from each other by hill-shaped barriers, 2) some local minima turn into local maxima.* This is displayed in Fig. 5. Per Conjecture 1, the former is explained by the bifurcation in the equilibrium number and the latter in that by which some stable equilibria become unstable.

Remark 1: Noteworthy, from (6) with $\bar{\tau} = 0$, the equilibrium pairs solve $\gamma H \bar{q} = -\Gamma(\bar{q})$. Due to oscillatory behavior at constant frequency and damped peaks of Γ_i (cf. e.g., Fig. 6), when moving away far enough from \bar{q} , it can be conjectured that the number of such solutions remains finite, except for $\gamma = 0$. However, this would imply a SIP with $k = 0$, $m \rightarrow \infty$, or $L \rightarrow \infty$, which is not physically attainable.

IV. STABILITY OF THE ZERO DYNAMICS RESULTING FROM COLLOCATED CONTROL STRATEGIES

Moving now to a control-oriented perspective, we immediately see that the SIP is structurally *underactuated* as it has two configuration variables and only one control variable. Referring to (1), q_0 is *collocated* with the actuation variable τ and q_1 is *non-collocated*. Accordingly, a feedback law $\tau = \tau(q_0, q_1, \dot{q}_0, \dot{q}_1)$ regulating q_0 to a desired value \bar{q}_0 is said to be a collocated control strategy, while one regulating q_1 is called non-collocated. Regardless of the choice, it is always necessary to prove the stability of the remaining dynamics, which forms the so-called internal zero-dynamics. Conveniently, the stability of such zero dynamics directly implies that of the overall system (cf. [20, Th. 1]).

We assume in the remainder that a *collocated control* law is realized, with the aim to stabilize the pendulum's tip orientation q_0 to the desired value \bar{q}_0 , and want to study the stability of all equilibria of the non-collocated q_1 . To do so, observe that a collocated control amounts to choosing the output function $y = q_0 - \bar{q}_0$ and to regulate it to zero. This is achieved for example via the feedback control law $\tau = K_{1,1}\bar{q}_0 + K_{1,2}\bar{q}_1 + G_1(\bar{q}_0, \bar{q}_1) - k_p(q_0 - \bar{q}_0) - k_d\dot{q}_0$, where k_p and k_d are positive control gains. Moreover, the expression of the second time-derivative of y contains the input variable τ , thus proving the existence of a zero dynamics since the SIP's relative degree ($r = 2$) is smaller than the dimension of its configuration space ($n = 4$). By zeroing y and its first two time derivatives, i.e., assuming $y = \dot{y} = \ddot{y} = 0$ for all times, gives $q_0 = \bar{q}_0$, $\dot{q}_0 = 0$, and $\ddot{q}_0 = 0$, which, plugged into the second relation of (1), leads to sought zero-dynamics:

$$B_{2,2}(\bar{q}_0, q_1)\ddot{q}_1 + C_{2,2}(\bar{q}_0, q_1)\dot{q}_1 + G_2(\bar{q}_0, q_1) + K_{2,1}\bar{q}_0 + K_{2,2}q_1 + \Delta_{2,2}\dot{q}_1 = 0. \quad (8)$$

A. Zero-Dynamics Equilibrium Pattern

We now characterize the equilibria of the zero-dynamics associated with a given collocated control. Knowledge of the control function is unnecessary, but it is assumed to be applied at all times to steer q_0 to \bar{q}_0 .

A zero-dynamics equilibrium is a constant solution $q_1(t) = \bar{q}_1$ of the differential model in (8). Plugging then $\dot{q}_1 = \ddot{q}_1 = 0$ into (8) gives $G_2(\bar{q}_0, q_1) + K_{2,1}\bar{q}_0 + K_{2,2}q_1 = 0$. Using, as above, the expressions $K_{2,1} = -6k$, $K_{2,2} = 12k$, and $G_2(\bar{q}_0, q_1) = mgL\Gamma_2(\bar{q}_0, q_1)$, the above is rewritten as

$$mgL\Gamma_2(\bar{q}_0, q_1) - 6k\bar{q}_0 + 12kq_1 = 0 \quad (9)$$

from which we deduce that the equilibria's existence and location depend both on the system parameters and the desired collocated variable value \bar{q}_0 . In this context, it is useful to try inferring the asymptotic behavior of the solutions of (9). To this purpose, rewrite (9) in the two equivalent forms:

$$\frac{\Gamma_2(\bar{q}_0, q_1)}{6\gamma} - \bar{q}_0 + 2q_1 = 0, \quad \Gamma_2(\bar{q}_0, q_1) + 6\gamma(2q_1 - \bar{q}_0) = 0. \quad (10)$$

The first relation allows concluding that for large enough γ ($\gamma \rightarrow \infty$), there is only one equilibrium that tends to the value $\bar{q}_1 = \frac{1}{2}\bar{q}_0$; from the second relation follows that, for small enough values of γ ($\gamma \rightarrow 0$), the equilibria converge to the solutions of $\Gamma_2(\bar{q}_0, q_1) = 0$. Referring to Fig. 6, where the functions $\xi = \Gamma_2(\bar{q}_0, q_1)$ and $\xi = 0$ (the horizontal plane) are plotted, we can see that, for $\gamma \rightarrow 0$, the equilibria become countably-infinitely many, and, given the desired \bar{q}_0 , they lay indeed at the intersections between the plotted functions and the line $q_0 = \bar{q}_0$.

For all intermediate values of γ and with $q_1 \neq \frac{1}{2}\bar{q}_0$, (9) is rewritten as $\gamma = \Gamma_2(\bar{q}_0, q_1)/(6\bar{q}_0 - 12q_1)$ which shows that

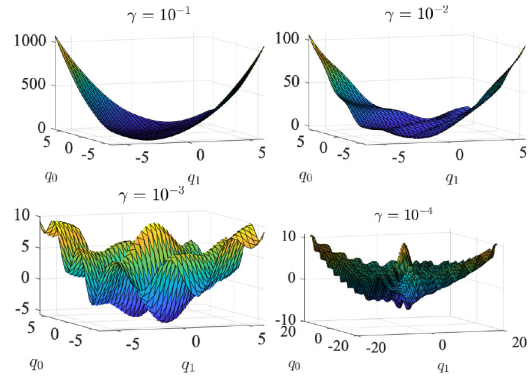


Fig. 5. Potential energy forms for various values of the bifurcation parameter γ . The figure highlights the radially unbounded behavior of U ; analytically speaking, while U_G is bounded via the Lagrangian description of the SIP [4], $U_K = \frac{1}{2}q^T Kq \rightarrow \infty$ for $\|q\| \rightarrow \infty$.

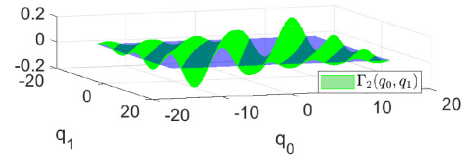


Fig. 6. Zero-dynamics equilibria for $\gamma \rightarrow 0$. The equilibria become countably-infinitely many and, given the desired value for the collocated variable, \bar{q}_0 , they tend to the intersections between the plotted functions and the line $q_0 = \bar{q}_0$.

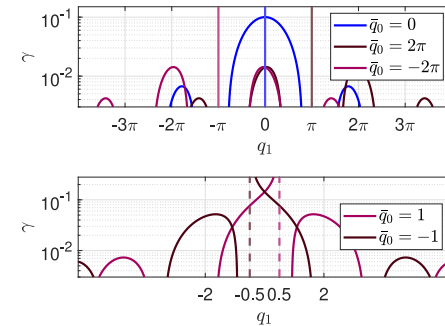


Fig. 7. Zero-dynamics equilibria for intermediate values of γ and various desired tip orientations \bar{q}_0 . Equilibria are found intersecting $\xi = \Gamma_2(\bar{q}_0, q_1)/(6\bar{q}_0 - 12q_1)$ and $\xi = \gamma$. The upper plot reports the graphs for $\bar{q}_0 \in \{-2\pi, 0, 2\pi\}$ and the lower one for $\bar{q}_0 \in \{1, -1\}$.

the equilibria are found by intersecting $\xi = \Gamma_2(\bar{q}_0, q_1)/(6\bar{q}_0 - 12q_1)$, with the horizontal line $\xi = \gamma$. If $q_1 = \frac{1}{2}\bar{q}_0$, the second relation in (10) indicates that $\Gamma_2(\bar{q}_0, \frac{1}{2}\bar{q}_0) = 0$. This occurs only for $\bar{q}_0 = 2\kappa\pi$, with $\kappa \in \mathbb{N}$. Three representative cases are depicted in Fig. 7 and relate to the SIP: 1) in the upright-position ($\bar{q}_0 = 0$), 2) surrounding an object ($\bar{q}_0 = 2\pi$), and 3) with a generic orientation ($\bar{q}_0 = 1$). For $\bar{q}_0 \in \{0, \pm 2\pi\}$, $\Gamma_2(\bar{q}_0, \frac{1}{2}\bar{q}_0) = 0$ always stands and so the equilibrium $\bar{q}_1 = \frac{q_0}{2}$ exists for all γ . The Cartesian SIP's shapes in some zero-dynamics equilibria are in Figs. 8 and 9.

B. Stability of Zero Dynamics Equilibria

A first insight into the stability of the zero-dynamics equilibria \bar{q}_1 when a collocated control law is applied to regulate q_0 to \bar{q}_0 , can be found in the following:

Proposition 3: A zero-dynamics equilibrium \bar{q}_1 is stable if, for all q_1 in a neighborhood of \bar{q}_1 , it holds

$$G_2(\bar{q}_0, q_1) + K_{2,1}\bar{q}_0 + K_{2,2}q_1 > 0. \quad (11)$$

Proof: Under the hypothesis in (11), the stability is proved by the Lyapunov function (and its time-derivative):

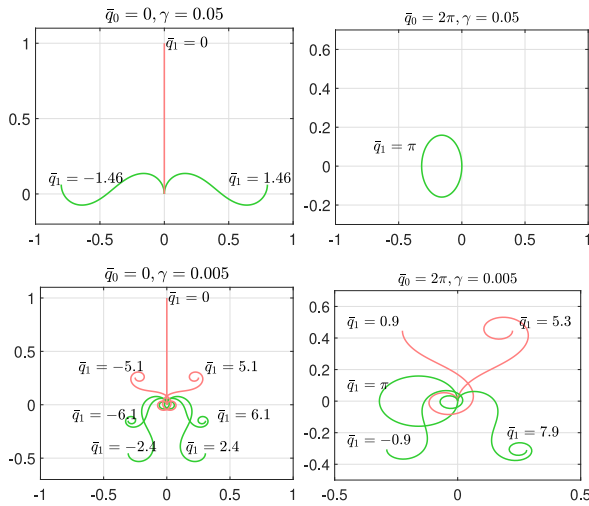


Fig. 8. Cartesian (x, y) shapes of the SIP at all zero-dynamics equilibria for $\bar{q}_0 \in \{0, 2\pi\}$ and $\gamma \in \{0.05, 0.005\}$. Abscissas and ordinates indicate x and y coordinates.

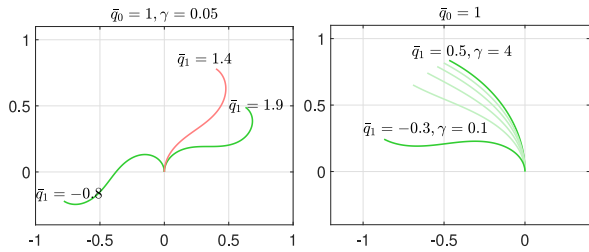


Fig. 9. Cartesian (x, y) shapes of the SIP with intermediate tip orientation ($\bar{q}_0 = 1$). The left plot displays the three possible zero-dynamics equilibria for $\gamma = 0.05$, while the right plot is intended to show how the unique equilibrium varies for values of $\gamma \geq 0.1$. Stable equilibria are in green and the unstable one is in red.

$$V = B_{2,2}(\bar{q}_0, q_1) \frac{\dot{q}_1^2}{2} + K_{2,2} \frac{q_1^2}{2} + \int_{\bar{q}_1}^{q_1} (G_2(\bar{q}_0, y) + K_{2,1}\bar{q}_0) dy,$$

$$\dot{V} = -\Delta_{2,2} \dot{q}_1^2 \leq 0.$$

The above derivative calculation uses the skew-symmetry of the matrices in (1) and Leibniz's integration rule by which

$$\begin{aligned} \frac{d}{dt} \int_{\bar{q}_1}^{q_1} (G_2(\bar{q}_0, y) + K_{2,1}\bar{q}_0) dy \\ = \frac{\partial}{\partial q_1} \int_{\bar{q}_1}^{q_1} (G_2(\bar{q}_0, y) + K_{2,1}\bar{q}_0) dy \dot{q}_1 \\ = (G_2(\bar{q}_0, q_1) + K_{2,1}\bar{q}_0) \dot{q}_1. \end{aligned}$$

As \dot{V} is only negative semi-definite, the proposition concludes only that the system is stable, but nothing is said about its asymptotic convergence to the equilibrium. ■

More conclusive results are obtained below exploiting Lagrange-Dirichlet's Theorem and [20, Th. 1], proving that underactuated systems' stability can be reduced to that of their zero-dynamics.

Proposition 4 (On Local Asymptotic Stability): The SIP's full model is locally asymptotically stable around a zero-dynamics equilibrium \bar{q}_1 if, for all q_1 in a neighborhood of \bar{q}_1 , it holds

$$\gamma > -\frac{1}{12} \frac{\partial}{\partial q_1} \Gamma_2(\bar{q}_0, q_1). \quad (12)$$

Proof: According to Lagrange-Dirichlet's Theorem, the local minima of the system's potential energy are Lyapunov-stable equilibria. This motivates the choice of the potential energy function

$$\begin{aligned} U(q_1) &= \int_{\bar{q}_1}^{q_1} (G_2(\bar{q}_0, y) + K_{2,1}\bar{q}_0) dy + \frac{1}{2} K_{2,2} q_1^2 \\ &= \int_{\bar{q}_1}^{q_1} (G_2(\bar{q}_0, y) + K_{2,1}\bar{q}_0 + K_{2,2}y) dy. \end{aligned}$$

All points (\bar{q}_0, \bar{q}_1) satisfying (9) make the first derivative of $U(q_1)$ with respect to q_1 vanish, meaning that they are extrema (minima or maxima) of $U(q_1)$. In fact, if the condition in (12) holds, they are minima since the second derivative of $U(q_1)$ with respect to q_1 is positive:

$$\frac{\partial^2 U}{\partial q_1^2} = \frac{\partial G_2(\bar{q}_0, q_1)}{\partial q_1} + K_{2,2} = mgL \frac{\partial \Gamma_2(\bar{q}_0, q_1)}{\partial q_1} + 12k > 0. \quad (13)$$

Under some stricter conditions, the following sufficient condition for global asymptotic stability can be proved:

Proposition 5 (On Global Asymptotic Stability): Under the same hypothesis of Prop. 4, the SIP's full model has a globally asymptotically stable equilibrium (\bar{q}_0, \bar{q}_1) , where \bar{q}_1 is the unique solution of (9), if

$$\gamma > \max_{q_1} \left(-\frac{1}{12} \frac{\partial}{\partial q_1} \Gamma_2(\bar{q}_0, q_1) \right). \quad (14)$$

Proof: The proof follows the steps of Prop. 4. In addition, since the function $-\frac{1}{12} \frac{\partial}{\partial q_1} \Gamma_2(\bar{q}_0, q_1)$ is bounded, its maximum exists. Then, when $\gamma = k/mgL$ is larger than such a maximum, as implied by (14), the concavity expression in (13) of the potential energy $U(q_1)$ never changes, which further implies that $U(q_1)$ has a unique extremum \bar{q}_1 that is the solution of (9) and that is a global minimum. ■

Finally, the following instability result can be provided:

Proposition 6 (On Instability): The SIP's full model is unstable around a zero-dynamics equilibrium \bar{q}_1 , if, for some q_1 arbitrarily close to \bar{q}_1 , it holds

$$\gamma < -\frac{1}{12} \frac{\partial}{\partial q_1} \Gamma_2(\bar{q}_0, q_1). \quad (15)$$

Proof: For all q_1 that are arbitrarily close to \bar{q}_1 and for which the condition in (15) holds, the condition on the second partial derivative of $U(q_1)$ in Prop. 4 holds with the negative sign. This implies that the first derivative $\frac{\partial U}{\partial q_1}(q_1)$ turns from being null at \bar{q}_1 (recall that \bar{q}_1 is a zero-dynamics equilibrium solving (9)) to a negative value, and, in turn, that \bar{q}_1 is either a saddle point or a (local) maximum for $U(q_1)$. Hence, small perturbations from \bar{q}_1 , along the direction where (15) holds, leads to divergence from the equilibrium. ■

Remark 2: Verifying (11) amounts to check if the sign of the scalar nonlinear function $G_2(\bar{q}_0, q_1) + K_{2,1}\bar{q}_0 + K_{2,2}q_1$ is positive $\forall q_1 \in [\bar{q}_1 - \eta, \bar{q}_1 + \eta]$, where $\eta > 0$ is a suited value to be (numerically) found. Similar reasoning holds for (12) and (15). More conveniently, we propose to prepare, for each \bar{q}_0 of interest, a chart allowing graphical determination of the number of equilibria (\bar{q}_0, \bar{q}_1) , the \bar{q}_1 coordinate, and their stability, for the γ of interest. An example of these charts is reported in Fig. 10. Given the charts, a SIP designer can simply draw a horizontal line for $\xi = \gamma$ to retrieve this data.

V. ENERGY-INJECTION SWITCHING CONTROL

We provide herein insights into a possible control strategy steering the SIP from one stable equilibrium to another. The collocated control law in [18] consisting of a partial feedback linearization and given by $\tau = h_1 - (B_{2,1}/B_{2,2})h_2 + (B_{1,1} - B_{2,1}^2/B_{2,2})u$ with $h = (h_1, h_2)^T = C(q, \dot{q})\dot{q} + G(q) + Kq + \Delta\dot{q}$ and $u = -k_p(q_0 - q_0^d) - k_d\dot{q}_0$, is used to let the SIP's tip orientation track a desired trajectory q_0^d .

The idea is to capitalize on the shape of the SIP's potential energy (Fig. 5) where stable equilibria are separated by "hill"

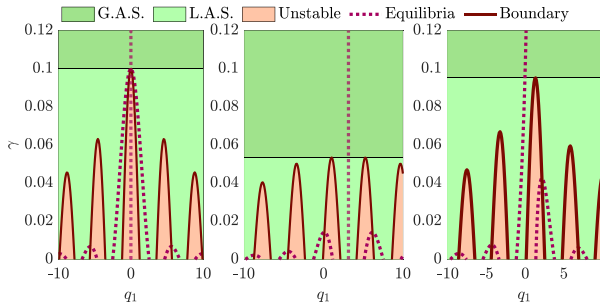


Fig. 10. Zero dynamics stability for a SIP in the upright-configuration ($\bar{q}_0 = 0$), completely surrounding an object ($\bar{q}_0 = 2\pi$), at an intermediate configuration ($\bar{q}_0 = 1$). The boundary is given by $\gamma = -\frac{1}{12} \frac{\partial \Gamma_2(\bar{q}_0, q_1)}{\partial q_1}$, which conservatively limits the global asymptotic stability region; also, the global asymptotic stability of zero-dynamics equilibria for $\bar{q}_0 = 2\pi$ is guaranteed for much lower values of γ , which intuitively implies that the SIP spiraling increases its stiffness.

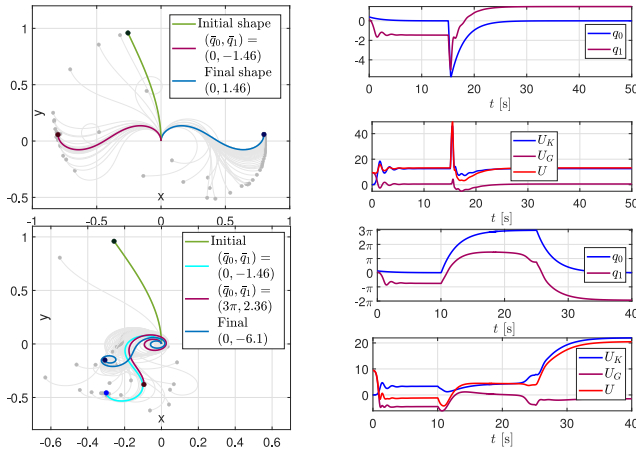


Fig. 11. Energy-injection-based control of SIP with $\gamma = 0.05$ (top) and $\gamma = 0.005$ (bottom). Left-side graphs show the SIP trace in the Cartesian coordinates as the SIP moves with time, top-right plots the temporal evolution of q_0 and q_1 , and bottom-right those of the potential energy terms (U_K , U_G , and U).

barriers, and to exploit Lagrange-Dirichlet's intuition for stability. Intuitively, one can tailor the reference q_0^d so as to inject additional energy into the SIP and allow it to reach the hills' top and end up in the region of attraction of a new equilibrium. This is done as in the swinging-up strategy of a pendulum [20], i.e., by setting $q_0^d = \alpha \arctan \dot{q}_1 + \beta$, with α and β suitable constants. Once the SIP enters the region of attraction of the new equilibrium, the stability is automatically guaranteed.

To exemplify this, consider first a SIP with $\gamma = 0.05$ and a desired null tip orientation ($\bar{q}_0 = 0$). In this case, there are two stable zero-dynamics equilibria in $m_1 = (0, -1.46)$ and $m_2 = (0, 1.46)$ (cf. Fig. 8). After letting the SIP move from an initial configuration $(q_0, q_1) = (0.4, 0.1)$ belonging to the region of attraction of m_1 to m_1 itself, the goal is to steer it towards m_2 . This is shown in Fig. 11 in which the collocated control gains are $k_p = 10$ and $k_d = 25$. Specifically, the collocated trajectory is initially chosen as $q_0^d = 25 \arctan \dot{q}_1$, which makes the SIP start swinging and straightening up, gradually injecting energy into it, and brings it to the side opposite to m_2 . As soon as the gravity potential energy in (3) is large enough, reaching the threshold $U_G = 4$, the reference signal is instantaneously set back to $q_0^d = \bar{q}_0 = 0$, which finally brings the SIP to m_2 .

To probe the strategy further, consider the richer case for $\bar{q}_0 = 0$ and $\gamma = 0.005$, including four stable equilibria $m_1 = (0, -2.4)$, $m_2 = (0, 2.4)$, $m_3 = (0, -6.1)$, $m_4 = (0, 6.1)$ (Fig. 8). As above, the SIP is first regulated to m_1 . Repeating

the same procedure in the previous paragraph can only bring the pendulum to the symmetrical m_2 , so to reach the equilibrium m_3 ; so, a two-step procedure needs to be followed. First the pendulum is set to swing with $q_0^d = 25 \arctan \dot{q}_1 + 3\pi$ until the gravity potential energy reaches $U_G = 1$. Then q_0^d is set to $q_0^d = 3\pi$, and the SIP makes a loop around its base. Finally, the tip orientation is brought back to $q_0^d = 0$ and the pendulum seizes equilibrium m_3 .

VI. CONCLUSION

This letter provided an in-depth analysis of the stability of a soft inverted pendulum with affine curvature, portraying how the equilibrium pattern and stability depend on its physical parameters. Choosing the collocated variable as the system's output, conditions were derived for zero-dynamics stability, local and global asymptotic stability, as well as instability. We leveraged these insights to design an energy-injection switching control law, steering the system among stable equilibria within the manifold of $q_0 = \bar{q}_0$. Future work will be devoted to the experimental verification of the proposed control strategy while, in our vision, the presented results will guide the development of control strategies for the more complex soft robots.

REFERENCES

- [1] C. D. Santina *et al.*, "Soft Robots," *Encyclopedia of Robotics*, M. H. Ang, O. Khatib, B. Siciliano, Eds. Berlin, Germany: Springer, 2020, pp. 1–15, doi: [10.1007/978-3-642-41610-1_146-2](https://doi.org/10.1007/978-3-642-41610-1_146-2)
- [2] T. G. Thuruthel *et al.*, "Control strategies for soft robotic manipulators: A survey," *Soft Robot.*, vol. 5, no. 2, pp. 149–163, 2018.
- [3] C. Armanini *et al.*, "Soft robots modeling: A literature unwinding," 2021, *arXiv:2112.03645*.
- [4] C. Della Santina *et al.*, "Model based control of soft robots: A survey of the state of the art and open challenges," 2021, *arXiv:2110.01358*.
- [5] R. J. Webster, III and B. A. Jones, "Design and kinematic modeling of constant curvature continuum robots: A review," *SAGE Int. J. Robot. Res.*, vol. 29, no. 13, pp. 1661–1683, 2010.
- [6] V. Falkenhahn *et al.*, "Model-based feedforward position control of constant curvature continuum robots using feedback linearization," in *Proc. Int. Conf. Robot. Autom.*, 2015, pp. 762–767.
- [7] C. D. Santina *et al.*, "Model-based dynamic feedback control of a planar soft robot: Trajectory tracking and interaction with the environment," *SAGE Int. J. Robot. Res.*, vol. 39, no. 4, pp. 490–513, 2020.
- [8] M. Trumic *et al.*, "Adaptive control of soft robots based on an enhanced 3D augmented rigid robot matching," in *Proc. Amer. Control Conf. (ACC)*, 2021, pp. 4991–4996.
- [9] M. Thieffry *et al.*, "LPV framework for non-linear dynamic control of soft robots using finite element model," *IFAC-PapersOnLine*, vol. 53, no. 2, pp. 7312–7318, 2020.
- [10] K. Wu and G. Zheng, "Fem-based gain-scheduling control of a soft trunk robot," *IEEE Robot. Autom. Lett.*, vol. 6, no. 2, pp. 3081–3088, Apr. 2021.
- [11] C. D. Santina and D. Rus, "Control oriented modeling of soft robots: The polynomial curvature case," *IEEE Robot. Autom. Lett.*, vol. 5, no. 2, pp. 290–298, Apr. 2020.
- [12] F. Boyer *et al.*, "Dynamics of continuum and soft robots: A strain parameterization based approach," *IEEE Trans. Robot.*, vol. 37, no. 3, pp. 847–863, Jun. 2021.
- [13] P. Pustina *et al.*, "Feedback regulation of elastically decoupled underactuated soft robots," *Robot. Autom. Lett.*, vol. 7, no. 2, pp. 4512–4519, Apr. 2022.
- [14] E. Franco and A. Garriga-Casanovas, "Energy-shaping control of soft continuum manipulators with in-plane disturbances," *Int. J. Robot. Res.*, vol. 40, no. 1, pp. 236–255, 2021.
- [15] B. J. Caasenbrood *et al.*, "Energy-based control for soft manipulators using Cosserat-beam models," in *Proc. 18th Int. Conf. Inf. Control Autom. Robot.*, 2021, pp. 311–319.
- [16] P. Borja *et al.*, "Energy-based shape regulation of soft robots with unactuated dynamics dominated by elasticity," in *Proc. Robosoft*, 2022, pp. 396–402.
- [17] L. Weerakoon and N. Chopra, "Swing up control of a soft inverted pendulum with revolute base," in *Proc. 60th Conf. Decis. Control (CDC)*, 2021, pp. 685–690.
- [18] C. D. Santina, "The soft inverted pendulum with affine curvature," in *Proc. 59th Conf. Decis. Control (CDC)*, 2020, pp. 4135–4142.
- [19] I. Fantoni and R. Lozano, *Non-Linear Control for Underactuated Mechanical Systems*. London, U.K.: Springer, 2002.
- [20] M. W. Spong, "Partial feedback linearization of underactuated mechanical systems," in *Proc. Int. Conf. Intel. Robots Syst. (IROS)*, vol. 1, 1994, pp. 314–321.